Stem Cell Reports
Article

ISSCR

OPEN ACCESS

Lineage Specification from Prostate Progenitor Cells Requires Gata3-Dependent Mitotic Spindle Orientation

Maxwell E.R. Shafer,[1,2] Alana H.T. Nguyen,[1] Mathieu Tremblay,[1,2] Sophie Viala,[1,2] Mélanie Béland,[1] Nicholas R. Bertos,[1] Morag Park,[1,2,3] and Maxime Bouchard[1,2,*]

[1]Rosalind and Morris Goodman Cancer Research Centre, McGill University, 1160 Pine Avenue West, Room 415, Montreal, QC H3A 1A3, Canada
[2]Department of Biochemistry, McGill University, 3655 Promenade Sir William Osler, Montreal, QC H3G 1Y6, Canada
[3]Departments of Medicine and Oncology, McGill University, Montreal, QC H4A 3T2, Canada
*Correspondence: maxime.bouchard@mcgill.ca
http://dx.doi.org/10.1016/j.stemcr.2017.02.004

SUMMARY

During prostate development, basal and luminal cell lineages are generated through symmetric and asymmetric divisions of bipotent basal cells. However, the extent to which spindle orientation controls division symmetry or cell fate, and the upstream factors regulating this process, are still elusive. We report that GATA3 is expressed in both prostate basal progenitor and luminal cells and that loss of GATA3 leads to a mislocalization of PRKCZ, resulting in mitotic spindle randomization during progenitor cell division. Inherently proliferative intermediate progenitor cells accumulate, leading to an expansion of the luminal compartment. These defects ultimately result in a loss of tissue polarity and defective branching morphogenesis. We further show that disrupting the interaction between PRKCZ and PARD6B is sufficient to recapitulate the spindle and cell lineage phenotypes. Collectively, these results identify a critical role for GATA3 in prostate lineage specification, and further highlight the importance of regulating spindle orientation for hierarchical cell lineage organization.

INTRODUCTION

The development of stratified epithelia requires precise coordination of morphogenetic and cell differentiation signals. The prostate epithelium is composed of secretory luminal cells surrounded by a layer of basal cells and interspersed by rare neuroendocrine cells. This epithelial bilayer is generated during development and maintained throughout adulthood (Marker et al., 2003). The hierarchy within and between these different cell types has recently been clarified both during development and in the adult prostate (Ousset et al., 2012; Wang et al., 2009, 2013; Wuidart et al., 2016), but much remains to be understood about the regulatory and molecular mechanisms of lineage specification.

During postnatal development of the prostate, the majority of prostatic bud growth and differentiation comes from progenitors within the basal lineage, contributing to the expansion and formation of both the basal and luminal lineages (Ousset et al., 2012; Pignon et al., 2013). Cell fate determination from basal progenitor cells is thought to rely largely on the orientation of cell division (Wang et al., 2014; Williams et al., 2014). Basal cells divide either symmetrically (parallel to the basement membrane), generating two daughter cells with a basal cell fate, or asymmetrically (perpendicular to the basement membrane), generating a basal and a luminal daughter cell (Wang et al., 2014). The transition from bipotent basal cells to the luminal fate can additionally proceed through the formation of "double-positive" ($CK5^+/CK8^+$) intermediate progenitor cells with unipotent luminal potential (Ousset et al., 2012; Xin et al., 2003). Once the prostate has formed, both basal and luminal cells are thought to be limited to unipotent divisions that maintain tissue homeostasis. Unipotent basal and luminal divisions also drive the majority of growth during regeneration of the tissue following castration (Choi et al., 2012; Liu et al., 2011). Evidence also exists for rare multipotent basal and luminal cells within the adult prostate (Choi et al., 2012; Liu et al., 2011; Wang et al., 2009, 2013; Xin et al., 2003).

Symmetric and asymmetric cell divisions are regulated by mitotic spindle orientation, which relies on the formation of a molecular bridge between the spindle poles and the lateral or apical membranes, respectively (Bergstralh and St Johnston, 2014). During asymmetric cell division, the spindle pole protein complex interacts with the apical polarity complex comprising the Par proteins Par3 (PARD3) and Par6 (PARD6B), and the protein kinase aPKC (PRKCZ and PRKCI) (Rodriguez-Boulan and Macara, 2014). During symmetric division, the dominant model is that PRKCZ prevents localization of the spindle pole to the apical membrane, leading to spindle pole attachment at the lateral membrane (Chatterjee and McCaffrey, 2014). These mechanisms have been proposed in several tissues, including the mammary gland, a system similar to the prostate. Intriguingly, very little is known about the regulation of these complexes (Ahmed and Macara, 2016).

We previously identified a role for the transcription factor Gata3 in prostate cancer (Nguyen et al., 2013). GATA3 expression is lost during cancer progression in both mouse and human prostates. In *Pten*-deficient mice, acute inactivation of *Gata3* accelerates prostate cancer progression,

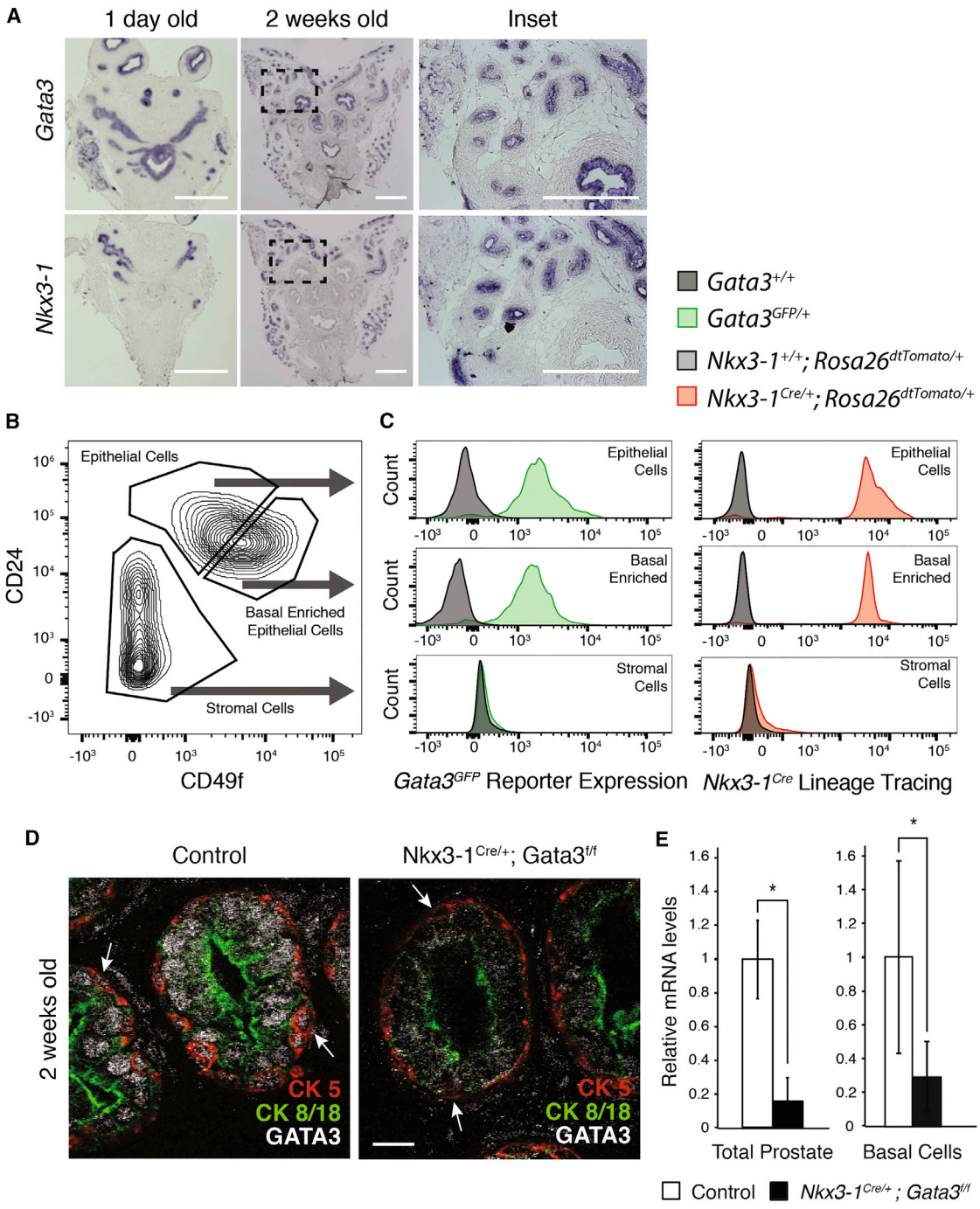

Figure 1. *Gata3* Is Expressed in Basal Cells during Prostate Development

(A) In situ hybridization of *Gata3* and *Nkx3-1* mRNA in newborn (1 day old) and postnatal (2 weeks old) prostate tissue. Insets show detection of mRNA in epithelial cells but not in surrounding stromal cells. Scale bars, 0.5 mm.

(B) Representative fluorescence-activated cell sorting (FACS) plot of prostate stromal, epithelial, and basal enriched cell populations from 2-week-old prostate tissue by CD24 and CD49f.

(C) Expression levels of endogenous $Gata3^{GFP}$ and $Nkx3\text{-}1^{Cre}$ activated $Rosa26^{dtTomato}$ lineage tracing reporters in the basal cell-enriched populations from 2-week-old prostate tissue. Wild-type and $Gata3^{GFP/+}$ mice, and $Nkx3\text{-}1^{Cre/+}$;$Rosa26^{dtTomato/+}$ and $Nkx3\text{-}1^{+/+}$; $Rosa26^{dtTomato/+}$ mice were used, respectively.

(legend continued on next page)

while its sustained expression delays the transition to carcinoma (Nguyen et al., 2013). Gata3 is also important for the specification and maintenance of many epithelial tissues including the epidermis and mammary gland, and is a recognized tumor suppressor in breast cancer (Asselin-Labat et al., 2007; Dydensborg et al., 2009; Kaufman et al., 2003). However, the role that *Gata3* plays during prostate development and in the generation and maintenance of epithelial polarity and homeostasis is poorly understood. Here, we show that *Gata3* regulates epithelial progenitor cell division via atypical protein kinase C (PRKCZ) to control lineage commitment during prostate development. This function of *Gata3* is achieved through precise regulation of spindle orientation in progenitor cells, disruption of which is sufficient to induce epithelial cell lineage and morphological defects.

RESULTS

Gata3 Is Required for Branching Morphogenesis and Epithelial Homeostasis during Prostate Development

We have previously shown that the transcription factor GATA3 plays a role in prostate cancer progression (Nguyen et al., 2013). To assess its role during prostate development, we first determined its precise expression pattern. In situ hybridization revealed specific expression of *Gata3* in the prostate epithelium (overlapping with *Nkx3-1* expression), in the urothelium of the bladder and in the seminal vesicles, whereas the urogenital mesenchyme was negative for *Gata3* (Figure 1A). To clarify which cell lineages expressed *Gata3* at 2 weeks of age, we performed fluorescence-activated cell sorting (FACS) using the surface markers CD24 and CD49f on prostate tissue from $Gata3^{GFP/+}$ knockin mice (Figure 1B). This confirmed that *Gata3* is expressed in all epithelial cells, including a basal cell-enriched epithelial population (Figure 1B), which also expresses *p63*, *CK5* and *CK14* (Figure S1).

To assess the functional role of *Gata3* during prostate development, we used the $Nkx3\text{-}1^{Cre}$ knockin mouse line in combination with a *Gata3* conditional knockout allele ($Gata3^{f/f}$) (Grote et al., 2006; Thomsen et al., 2008) (Figure S1B). Although it is later restricted to the luminal compartment, $Nkx3\text{-}1^{Cre}$ is expressed in both basal and luminal lineages during early development and efficiently activated the $Rosa26^{dtTomato}$ lineage tracer allele in the basal enriched $CD24^{+}$;$CD49f^{+}$ cell population at 2 weeks of age (Figure 1C) (Wu et al., 2011). Exon 4 of *Gata3* is also deleted by $Nkx3\text{-}1^{Cre}$ in both lineages at 2 weeks of age, leading to a loss of GATA3 protein in basal and luminal cells (Figures 1D and 1E). To visualize branching morphogenesis of the developing prostate, we took advantage of the $Rosa26R^{LacZ}$ reporter allele (Soriano, 1999), which was effectively activated in the prostate epithelium of $Nkx3\text{-}1^{Cre}$;$R26R^{LacZ}$ mice. At 2 weeks of age, *Gata3*-deficient prostates were smaller than control prostates and harbored less complex branching patterns, with significantly fewer ductal tips and branching points (Figures 2A and 2B). Similar smaller prostates and defective ductal architecture were also observed at 6 weeks of age (Figure S2). Cross-sections from 2- to 6-week-old *Gata3*-deficient prostates showed hyperplasia of the epithelial compartment as compared to control animals (Figures 2C and 2D). This was associated with an increase in proliferation (phospho-histone H3 marks), but no significant changes in cell death (TUNEL) (Figure 2E). Together, these results point to an important role for *Gata3* in prostate development.

Gata3 Deficiency Leads to Disorganization of Epithelial Polarity and an Accumulation of Intermediate Progenitor Cells

We next assessed whether disrupted prostate epithelial architecture induced by loss of *Gata3* affected apical/basal cell polarity. In wild-type prostate epithelial cells, E-cadherin localizes to the basal-lateral domain and ZO-1 marks tight junctions on the apical domain (Figure 3A). Interestingly, hyperplastic regions of *Gata3*-deficient prostates showed an accumulation of non-polarized cells, evidenced by expression of E-cadherin throughout the cell membrane (Figure 3A). *Gata3*-deficient luminal cells maintained ZO-1 localization and apical-basal expression of E-cadherin, indicating that they retained the ability to form a polarized epithelial layer. This staining further revealed the formation of ectopic lumens within hyperplastic regions of the epithelium (Figure 3A, inset).

In the absence of major defects in cellular apical-basal polarity within the luminal lineage, the observed epithelial defects could be caused by an effect on lineage specification from progenitor cells. To identify cell lineage defects within the prostate, we assessed the number of single-positive basal cells ($CK5^{+}$), single-positive luminal cells ($CK8/18^{+}$), or double-positive intermediate progenitor cells

(D) Immunohistochemistry against GATA3 protein in luminal ($CK8/18^{+}$) and basal ($CK5^{+}$) epithelial cells. Arrows indicate expression of GATA3 in basal cells. Scale bar, 5 μm.

(E) qRT-PCR detection of *Gata3* mRNA in total and FACS enriched basal cells from control and $Nkx3\text{-}1^{Cre/+}$;$Gata3^{flox/flox}$ mice. Expression levels displayed are relative to control tissue and corrected on housekeeping Ppia expression levels. Representative images and quantifications are from four control and three $Nkx3\text{-}1^{Cre/+}$;$Gata3^{flox/flox}$ prostates and independent sorted populations. *$p < 0.05$.

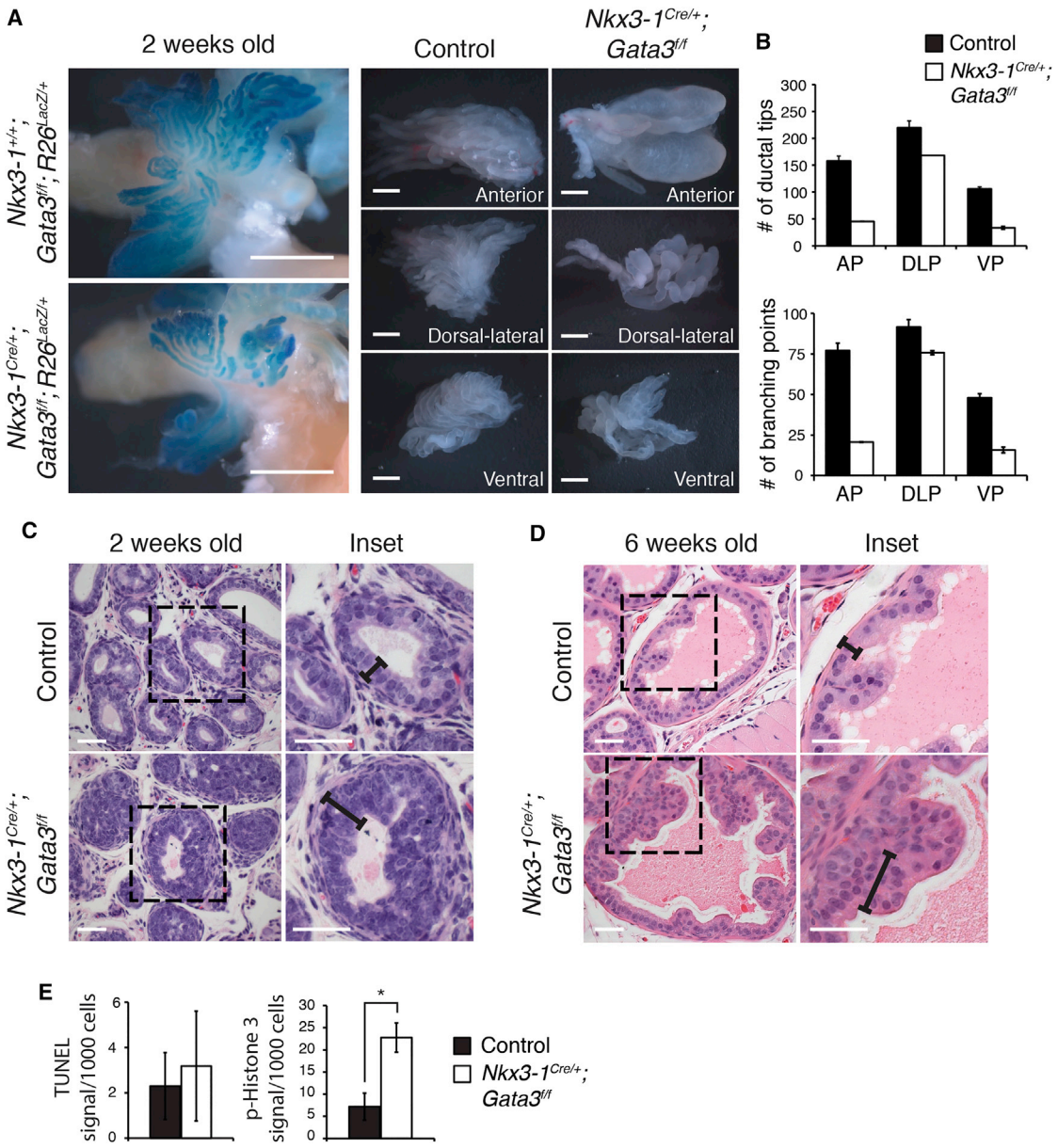

Figure 2. *Gata3* Is Required for Branching Morphogenesis and Prostate Epithelial Homeostasis

(A) Ductal architecture of control and *Nkx3-1*$^{Cre/+}$;*Gata3*$^{flox/flox}$ prostates and individual lobes at 2 weeks of age as shown by β-galactosidase staining. Scale bars, 1 mm.

(B) Quantification of the number of prostate ducts and branch points in control and *Nkx3-1*$^{Cre/+}$;*Gata3*$^{flox/flox}$ prostates.

(C) H&E staining of developing (2-week-old) prostate sections in control and *Nkx3-1*$^{Cre/+}$;*Gata3*$^{flox/flox}$ mice. Scale bars, 20 μm.

(D) H&E staining of developing (6-week-old) prostate sections in control and *Nkx3-1*$^{Cre/+}$;*Gata3*$^{flox/flox}$ mice. Black bars indicate the thickness of the epithelial layer. Scale bars, 20 μm.

(E) Quantification of proliferating (phospho-histone H3-positive cells) and apoptotic (TUNEL staining) cells in control and *Nkx3-1*$^{Cre/+}$; *Gata3*$^{flox/flox}$ tissue at P14. *$p < 0.05$.

Representative images and quantifications are from three control and *Nkx3-1*$^{Cre/+}$;*Gata3*$^{flox/flox}$ prostates, except in (B), where error bars represent SE from two control and *Nkx3-1*$^{Cre/+}$;*Gata3*$^{flox/flox}$ prostates.

(CK5$^+$; CK8/18$^+$) in both control and *Gata3*-deficient 2-week-old prostate tissue by immunohistochemistry (IHC). This analysis revealed that epithelial hyperplasia was caused by an increase in the number of intermediate progenitor and luminal cells, while the number of single-positive basal cells was not significantly affected

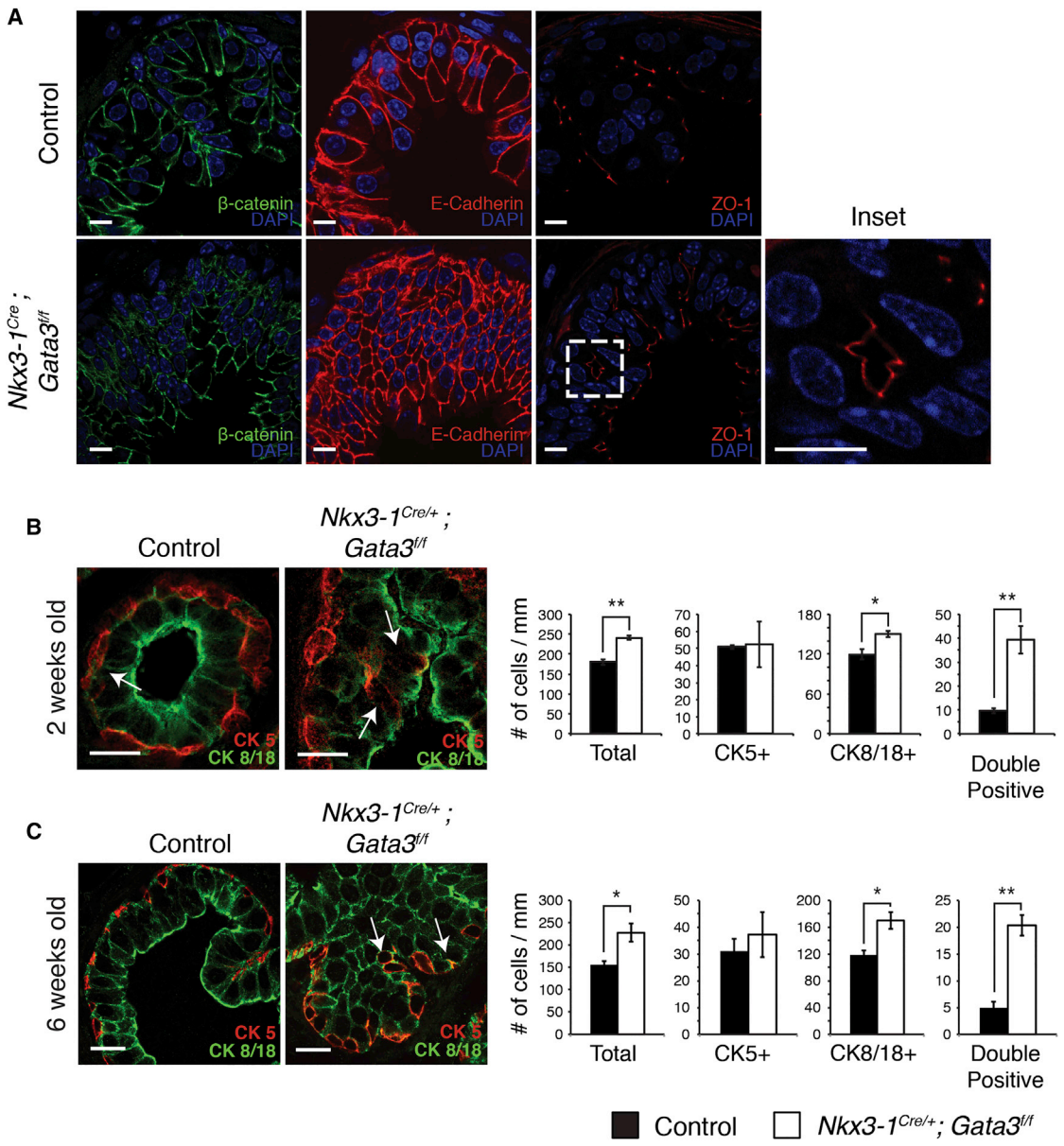

Figure 3. Loss of *Gata3* Disrupts Prostate Epithelial Polarity and Increases the Double-Positive Progenitor Cell Population

(A) Immunofluorescence staining of basolateral (B-catenin and E-cadherin) and apical (ZO-1) markers in control and *Nkx3-1*$^{Cre/+}$; *Gata3*$^{flox/flox}$ prostate tissue.

(B) Immunofluorescence staining of basal (CK5) and luminal (CK8/18) cell markers in 2-week-old control and *Nkx3-1*$^{Cre/+}$;*Gata3*$^{flox/flox}$ prostate and quantification of the number of single-positive basal (CK5^{+}), luminal (CK8/18^{+}), and double-positive intermediate progenitor (CK5^{+}; CK8/18^{+}) cells per millimeter of ductal circumference.

(C) Immunofluorescence staining of basal (CK5) and luminal (CK8/18) cell markers in 6-week-old control and *Nkx3-1*$^{Cre/+}$;*Gata3*$^{flox/flox}$ prostate and quantification of the number of single-positive basal (CK5^{+}), luminal (CK8/18^{+}), and double-positive intermediate progenitor (CK5^{+}; CK8/18^{+}) cells per millimeter of ductal circumference. Arrows in (B and C) indicate double-positive cells.

*$p < 0.05$, **$p < 0.01$. Representative images and quantifications are from four control and *Nkx3-1*$^{Cre/+}$;*Gata3*$^{flox/flox}$ prostates. Error bars represent SE from three (B) and four (C) control and *Nkx3-1*$^{Cre/+}$;*Gata3*$^{flox/flox}$ prostates. Scale bars, 10 μm.

(Figure 3B). Analysis of 6-week-old prostates revealed a similar accumulation of intermediate progenitor cells (Figure 3C). In addition, double-positive cells were found throughout both the basal and luminal compartments in *Gata3*-deficient prostates, in contrast to their typical basal location in control tissue. Together, these results identify

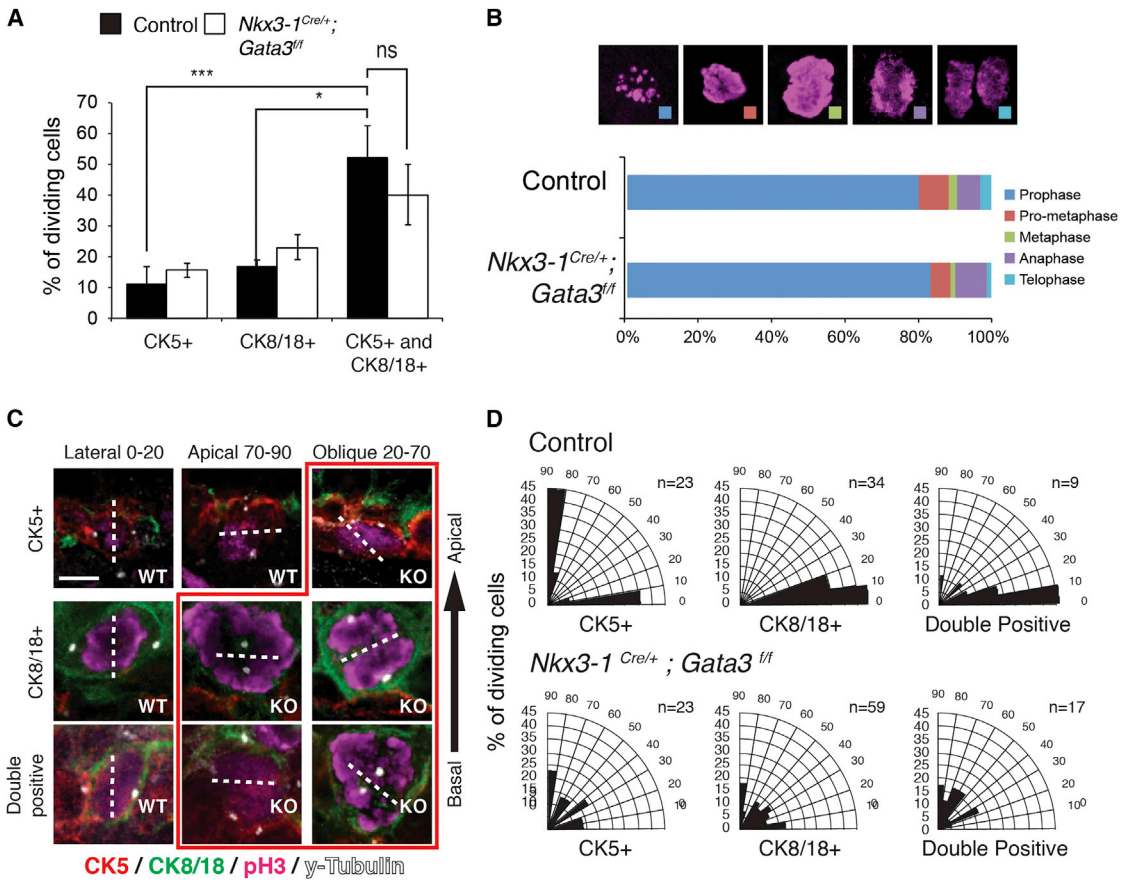

Figure 4. Loss of *Gata3* Randomizes Spindle Orientation in Basal Progenitor Cells without Affecting Their Proliferation Rate

(A) Percentage of dividing cells in each epithelial lineage in control and *Nkx3-1*$^{Cre/+}$;*Gata3*$^{flox/flox}$ prostate tissue.

(B) Analysis of the phases of mitosis in control and *Nkx3-1*$^{Cre/+}$;*Gata3*$^{flox/flox}$ prostate tissue.

(C) Mitotic spindle orientation was measured in basal (CK5$^+$), luminal (CK8/18$^+$), and double-positive cells (CK5$^+$; CK8/18$^+$) of control and *Nkx3-1*$^{Cre/+}$;*Gata3*$^{flox/flox}$ (red box) prostate tissue by γ-tubulin (spindle poles) and phospho-histone H3 (dividing cells) immunofluorescence staining.

(D) Quantification of spindle orientations in the three cell types in control and *Nkx3-1*$^{Cre/+}$;*Gata3*$^{flox/flox}$ prostate.

Dashed lines indicate axis of cytokinesis. *$p < 0.05$, ***$p < 0.001$; ns, not significant. Quantifications are from four control and *Nkx3-1*$^{Cre/+}$;*Gata3*$^{flox/flox}$ prostates. Error bars in (A) represent SE from four control and *Nkx3-1*$^{Cre/+}$;*Gata3*$^{flox/flox}$ prostate replicates. n values in (D) represent the total number of cell divisions quantified per cell type. Scale bars, 5 μm.

a crucial role for *Gata3* in establishing tissue architecture and lineage specification during prostate development.

Gata3 Deficiency Leads to Spindle Orientation Defects

These changes in cell lineage composition raised the intriguing possibility that the hyperplasia of *Gata3* mutant prostates may be caused by the increase in the population of intermediate progenitor cells rather than an increase in the proliferation rate of *Gata3*-deficient cells. To test this we measured the number of proliferative basal, luminal, and double-positive cells, controlling for the size of each population. This analysis revealed a 3- to 5-fold higher proliferation rate of intermediate progenitors relative to single-positive cells in wild-type prostates (Figure 4A). However, the proliferation rate and cell-cycle progression of *Gata3*-deficient cells were unchanged compared with controls (Figures 4A and 4B). This important result shows that the hyperplastic phenotype, and increased luminal cell numbers, results from an increase in intermediate progenitor specification rather than a defect in proliferation control of *Gata3*-deficient prostatic epithelial cells.

Given the correlation between spindle orientation and prostate lineage specification (Wang et al., 2014), we reasoned that the increase in double-positive intermediate progenitors could be secondary to a defect in the regulation of oriented cell division in basal cells. To identify dividing cells and the orientation of their spindle poles, we co-stained prostates for CK5 and CK8/18 (basal and luminal

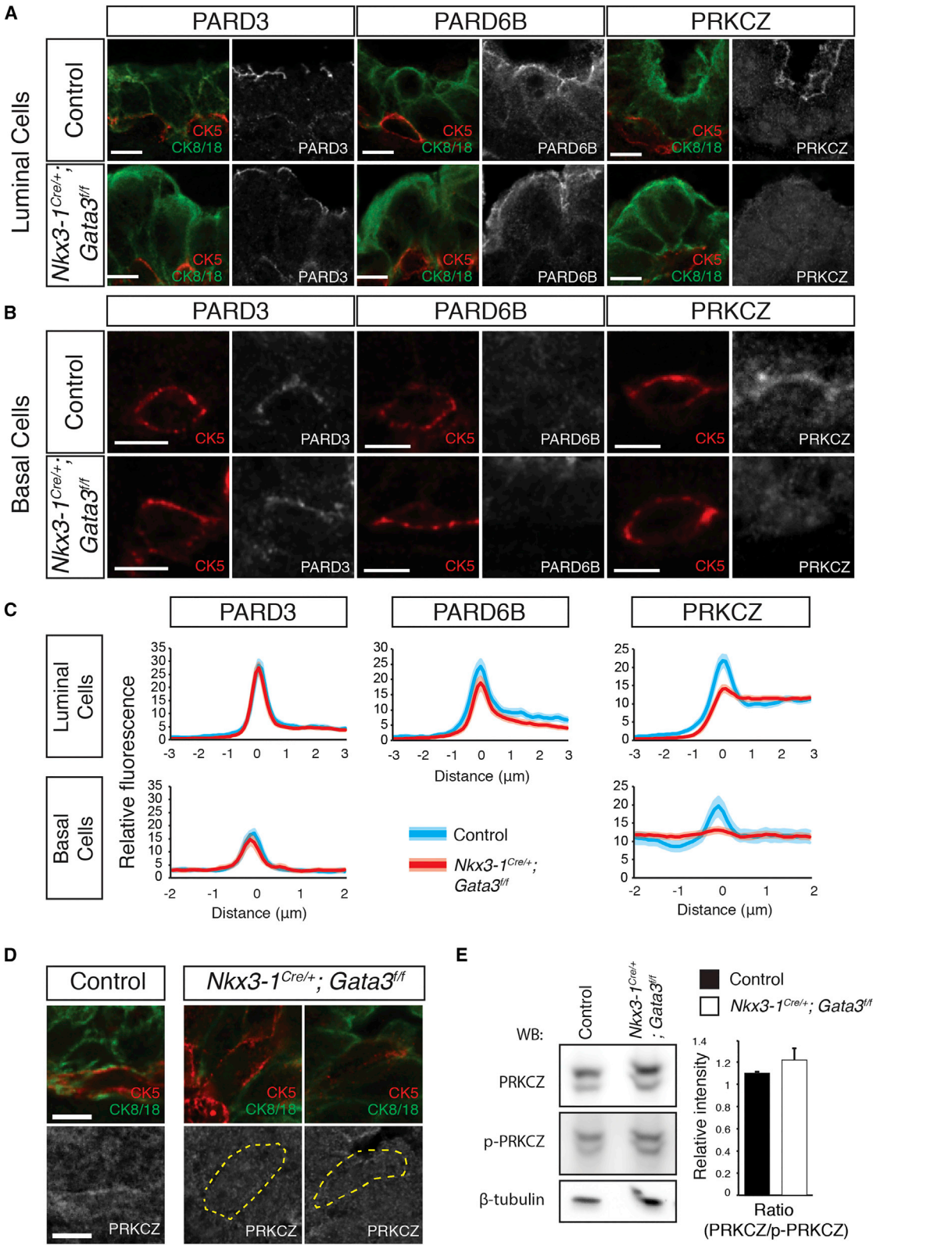

(legend on next page)

markers, respectively), γ-tubulin (spindle poles), and phospho-histone H3 to mark mitotic cells (mother cells during metaphase/anaphase or daughter cells during telophase). This analysis in control prostate tissues at 2 weeks of age confirmed that basal cells divide both vertically (basal-luminal) or horizontally (within the cell layer), whereas luminal cells only divide horizontally (Figures 4C and 4D). Strikingly, in the absence of *Gata3*, both the basal and luminal cell division angles were randomized (Figures 4C and 4D). In addition, γ-tubulin staining revealed a centrosome positioning defect in basal cells during interphase, which is a marker of polarization within these cells (Figure S3). Together, these results indicate that *Gata3* is required for mitotic spindle orientation and that spindle randomization may lead to lineage specification defects.

Gata3 Is Necessary for Normal PRKCZ Subcellular Localization in Basal and Luminal Cells

The apically localized Par complex is critical for the establishment and maintenance of epithelial cell polarity and for mitotic spindle orientation during symmetric/asymmetric cell division (Rodriguez-Boulan and Macara, 2014). We determined the subcellular localization of Par complex components PARD3, PARD6B, and PRKCZ by IHC. PARD3 and PARD6B were specifically localized to the apical domains in both wild-type and *Gata3* null luminal cells (Figure 5A). PARD3 was also detected in basal cells, and was localized to the apical membrane in both control and *Gata3* null tissue (Figure 5B), while the PARD6B isoform was not detected in basal cells (Figure 5B). Importantly, PRKCZ, which localized to the apical membrane of both luminal and basal cells in control ducts, failed to do so in *Gata3*-deficient prostates (Figures 5A and 5B). Measurements of fluorescence across the apical membrane (from apical side to nucleus) revealed a significant decrease in apical accumulation of PRKCZ in both cell types, leading to a diffuse staining in the cytoplasm (Figure 5C). To confirm this result and rule out any phenotypic contribution of *Nkx3-1* heterozygosity in *Nkx3-1*$^{Cre/+}$;*Gata3*$^{f/f}$ mice, we derived embryonic day 18.5 urogenital sinuses (UGS) by chemical rescue of germline *Gata3* mutant embryos (Kaufman et al., 2003; Lim et al., 2000) and implanted them under the kidney capsule of immunodeficient mice for 2 weeks (Figure S4A). Immunohistochemical analysis of UGS derivative tissues showed normal PARD3 and PARD6B expression but mislocalization of PRKCZ in both prostate and seminal vesicle epithelial cells (Figures S4D–S4E).

To determine whether the mislocalized PRKCZ is still active in *Gata3*-deficient prostates, we next assessed the amount of total and phosphorylated PRKCZ (phosphoT560) by western blot. This analysis revealed no differences in total or active PRKCZ between control and *Gata3* null prostates (Figure 5D), indicating that *Gata3* regulates PRKCZ localization without affecting its activation potential.

We next assessed the transcriptional consequences of *Gata3* deficiency by microarray analysis of laser captured prostate epithelial tissue from control and *Gata3*-deficient prostates (Figure S5, Table S1, and Data S1). This analysis revealed major effects on the secretory function of the prostate (secreted, signal, disulfide bond, extracellular matrix, glycoprotein), and on genes involved in immunity, most likely reflective of the known functions of GATA3 (Figure S5B). However, no obvious mediators of PRKCZ subcellular localization were identified.

Mislocalization of PRKCZ Is Sufficient to Cause Spindle Orientation and Lineage Specification Defects

To assess whether the misregulation of the polarity regulator PRCKZ was sufficient to generate spindle orientation defects, we made use of the small molecule aurothiomalate (ATM), which inhibits the interaction between PRKCZ and PARD6B by specifically binding to the PB1 domain of PRKCZ (Erdogan et al., 2006). Treatment with ATM has been successfully used to disrupt asymmetric cell division in T cells (Oliaro et al., 2010). We initially used Caco-2 cells, which are a well-established model of epithelial morphogenesis and form highly polarized cysts that exhibit strictly planar/symmetric divisions, which are reliant upon PRKCZ (Durgan et al., 2011). Strikingly, ATM treatment led to a randomization of mitotic spindle orientation and a decrease in the formation of hollow cysts accompanied by an increase in the incidence of cysts with multiple lumens (Figure S6). These results

Figure 5. *Gata3* Controls PRKCZ Localization in Prostate Basal and Luminal Cells

(A) Immunofluorescence of PARD3, PARD6B, and PRKCZ in luminal cells of control and *Nkx3-1*$^{Cre/+}$;*Gata3*$^{flox/flox}$ prostates.

(B) Immunofluorescence of PARD3, PARD6B, and PRKCZ in basal cells of control and *Nkx3-1*$^{Cre/+}$;*Gata3*$^{flox/flox}$ prostates.

(C) Quantification of PARD3, and PRKCZ fluorescence intensity across the apical membrane in luminal and basal cells measured from the lumen (−3/2) to the nucleus (+3/2), and quantification of PARD6B localization in luminal cells.

(D) Example immunofluorescence images of CK5, CK8/18, and PRKCZ staining in double-positive intermediate cells. Dashed lines indicate the periphery of double-positive cells.

(E) Western blot of PRKCZ and T-560 phosphorylated PRKCZ from control and *Nkx3-1*$^{Cre/+}$;*Gata3*$^{flox/flox}$ mice.

Images are representative of results from five control or *Nkx3-1*$^{Cre/+}$;*Gata3*$^{flox/flox}$ prostates, and quantification is from three control and *Nkx3-1*$^{Cre/+}$;*Gata3*$^{flox/flox}$ prostates (thickness of lighter red and blue bands represent SD from the mean). Scale bars, 5 μm.

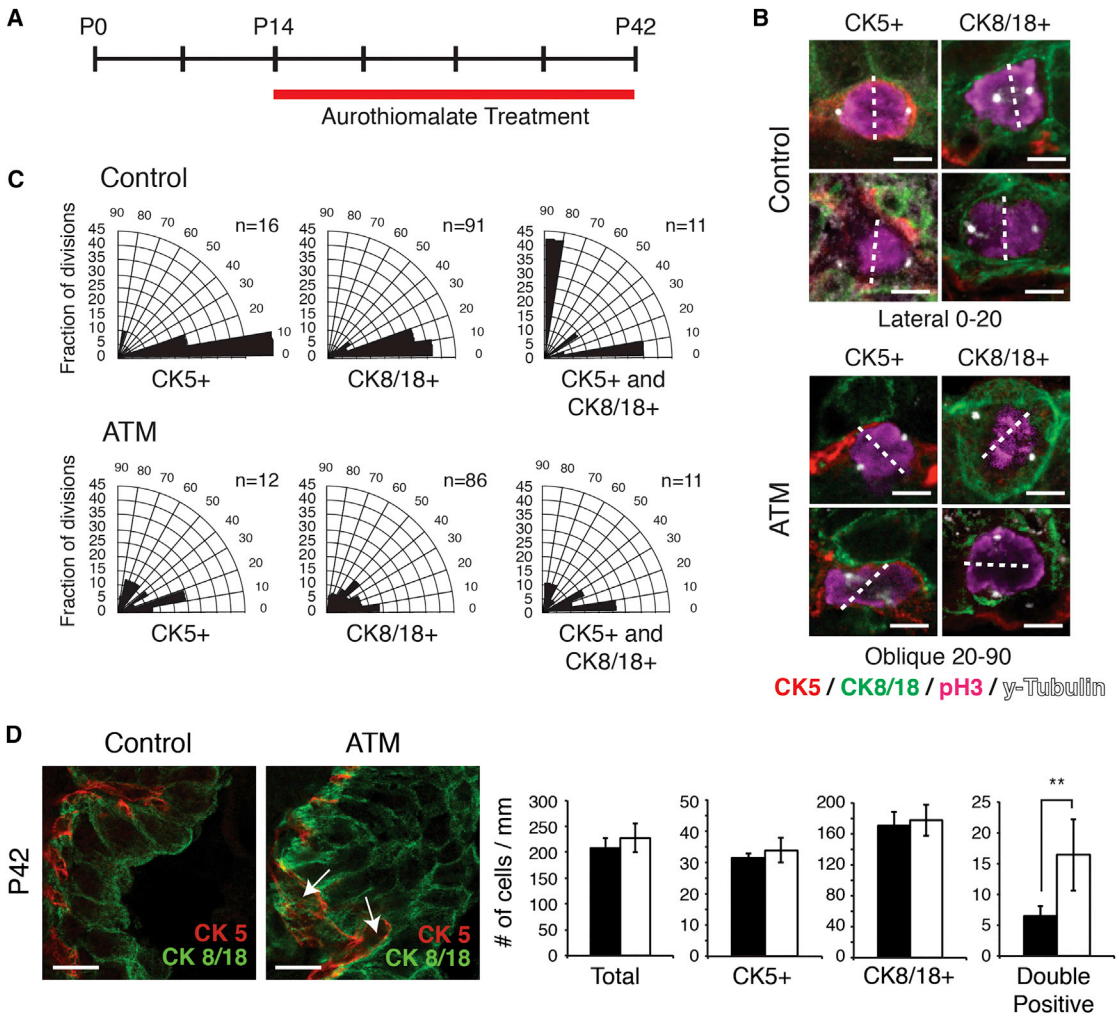

Figure 6. Disruption of PRKCZ-PARD6B Interaction Increases the Population of Double-Positive Intermediate Progenitor Cells in the Developing Prostate

(A) Timeline of ATM administration to adolescent male mice.

(B) Representative examples of spindle orientations in control or ATM-treated prostates at 6 weeks old. Dashed lines indicate axis of cytokinesis.

(C) Quantification of mitotic spindle orientation measured in basal ($CK5^+$), luminal ($CK8/18^+$), and double-positive cells ($CK5^+$; $CK8/18^+$) in control and ATM-treated prostate tissue. Spindle orientation was revealed by γ-tubulin (spindle poles) and phospho-histone H3 (dividing cells) immunofluorescence staining.

(D) Immunofluorescence of control and ATM-treated prostates, and quantification of the number of single-positive basal ($CK5^+$), luminal ($CK8/18^+$), and double-positive progenitor ($CK5^+$; $CK8/18^+$) (arrows) cells in control and ATM-treated prostates. $^{**}p < 0.01$.

Representative images and quantifications are from four control and four ATM-treated prostates. n values in (C) represent the total number of cell divisions quantified per cell type. Scale bars, 5 μm (B) and 10 μm (D).

suggest that apical PRKCZ-PARD6B interaction is important for proper mitotic spindle orientation and epithelial morphogenesis.

We next asked whether the PRKCZ-PARD6B interaction was necessary for mitotic spindle regulation and lineage specification in vivo. To this end, we treated adolescent male mice with ATM for 4 weeks during prostate development (Figure 6A). At 6 weeks of age, control and ATM-treated prostates were dissected, and both spindle orientation and epithelial lineage specification were analyzed. As expected, both basal and luminal cells of control animals divided strictly symmetrically, parallel to the duct, consistent with their established unipotency at this stage (Figures 6B and 6C) (Wuidart et al., 2016). Strikingly, ATM treatment was sufficient to randomize the mitotic spindle in both basal and luminal cells (Figures 6B and 6C), and

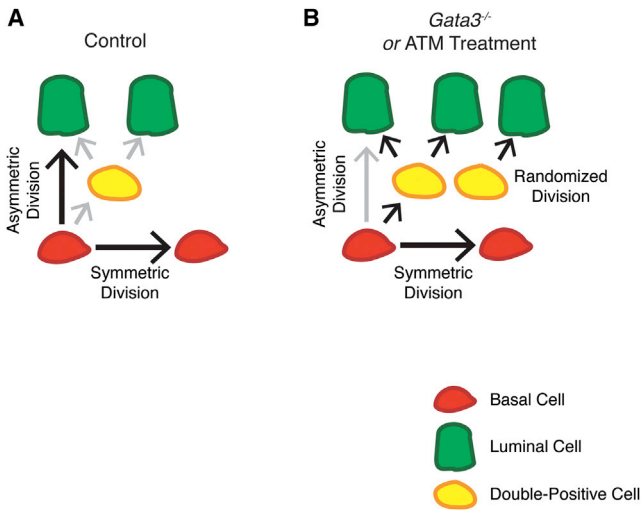

Figure 7. Control of Lineage Specification and Cell-Type Stratification during Prostate Development

(A) During normal prostate development, basal (red) cells generate both the basal and luminal lineages using symmetric and asymmetric cell divisions. In addition, double-positive cells (yellow) are generated from basal cells and contribute to the formation of the luminal lineage (green).

(B) Upon loss of *Gata3* or treatment with ATM, spindle orientation is randomized, leading to an increase in the number of intermediate progenitor cells. Increased intermediate progenitor cells contribute to an expanded luminal layer and prostate epithelial hyperplasia.

randomization of the mitotic spindle during prostate development caused a significant increase in the population of double-positive progenitor cells compared with control prostates (Figure 6D). These results demonstrate that spindle orientation is required for proper lineage specification from basal prostate epithelial cells, and highlight the critical importance of PRKCZ regulation during prostate development (Figure 7).

DISCUSSION

Basal prostate epithelial cells divide either symmetrically to expand the basal progenitor cell pool, or asymmetrically to generate double-positive intermediate progenitor cells or differentiated luminal cells (Ousset et al., 2012; Wang et al., 2013; Wuidart et al., 2016). However, the molecular determinants underlying this process and the consequences of altering spindle orientation in the prostate are currently unknown. In this report we show that loss of *Gata3* leads to tissue hyperplasia by accumulation of a poorly polarized cell layer at the interphase between the basal and luminal cells, largely composed of intermediate progenitor cells. This disruption in tissue architecture results from a defect in mitotic spindle orientation secondary to mislocalization of the polarity protein PRKCZ from PARD3/PARD6B. Accordingly, disruption of the PRKCZ-PARD6B interaction by ATM alone was sufficient to disrupt spindle orientation and lineage specification. Together, these results underscore the critical importance of regulating spindle orientation within progenitor cells to generate and maintain stable tissue architecture composed of stratified basal and luminal cell layers.

The most striking phenotype observed in *Gata3*-deficient prostates is a complete randomization of the mitotic spindle in both basal and luminal cells. In other systems, orientation of the mitotic spindle is recognized as the primary endogenous mechanism to regulate symmetric versus asymmetric cell divisions and control the inheritance of cellular fates within the resulting daughter cells (Knoblich, 2010; Morin and Bellaiche, 2011; Neumuller and Knoblich, 2009). This developmental program and its regulatory machinery are largely conserved during evolution, but little is known of the role of spindle and polarity proteins during development and homeostasis (Pearson et al., 2011; Win and Acevedo-Duncan, 2008; Zhang et al., 2016). Evidence from lineage tracing analysis and measurements of the mitotic spindle during lineage specification strongly support the presence of bipotent basal progenitor cells able to expand the basal compartment via laterally oriented divisions, or generate differentiated luminal cells via apical-oriented divisions (Ousset et al., 2012; Wang et al., 2014). Generation of luminal cells is partially accomplished through the formation of intermediate progenitors with a "double-positive" ($CK5^+$; $CK8/18^+$) signature. In contrast, luminal cells appear to be strictly unipotent and only capable of planar-oriented divisions during development and homeostasis. Importantly, this differentiation process occurs in a highly regulated manner such that prostatic ducts maintain stratified and single-cell thick layers of basal and luminal cells following mitotic events. In *Gata3*-deficient embryos, mitotic spindle randomization does not overtly affect the basal progenitor pool or the polarity of differentiated non-proliferative cells lining the lumen. Instead, it affects the relative allocation of the different lineages by accumulation of intermediate progenitor cells at the interphase between the differentiated basal and luminal cell compartments. These progenitor cells, along with oblique and apical divisions of luminal cells, disrupt tissue architecture by generating a surplus of luminal cells. Although we cannot exclude the possibility that some double-positive cells arise from aberrant luminal cell divisions, the fact that we observe spindle randomization in basal cell progenitors indicates disruption of the normal specification process in those cells.

We also find that PRKCZ fails to accumulate normally at the apical membrane in *Gata3* mutant embryos, even

though its expression and activation levels are maintained. PRKCZ is part of the apical Par complex comprising PARD3 and PARD6B and acts as a key regulator of mitotic spindle orientation in other systems (Durgan et al., 2011; Guilgur et al., 2012; Niessen et al., 2013). Of interest, the subcellular redistribution of PRKCZ is found in the presence of normal PARD3 and PARD6B apical expression, suggesting a decoupling of PRKCZ from the Par complex. Very few examples of such a decoupling phenotype have been documented so far. Only loss of Patj (*Inadl*) in MDCK cells or *Dlg5* during mouse lung development have been associated with a mislocalization of PRKCZ, possibly through PARD3 and PARD6B protein misexpression, which is not observed upon *Gata3* loss (Adachi et al., 2009; Nechiporuk et al., 2013; Shin et al., 2005). The detailed mechanisms by which loss of *Gata3* leads to PRKCZ mislocalization will require further investigation.

Using ATM, a small molecule that affects the interaction between PRKCZ and the Par complex (Erdogan et al., 2006), we showed that PRKCZ decoupling from PARD6B is sufficient to cause mitotic spindle orientation and epithelial defects. This is in line with the known role of PRKCZ as a kinase for spindle pole proteins (Hao et al., 2010). Phosphorylation by apical PRKCZ has been proposed to prevent spindle machinery from interacting with the apical domain, thereby preventing asymmetric cell division (Chatterjee and McCaffrey, 2014; Hao et al., 2010). Together, our results suggest a model by which the mislocalization of PRKCZ by loss of *Gata3* leads to spindle randomization by ectopic inhibition of the interaction between astral microtubules and the cell cortex (Figure 7).

The epithelial hyperplasia resulting from spindle randomization is likely to be an important underlying cause of the branching morphogenesis defects observed in *Gata3*-deficient prostates. Hyperplastic tissue remained epithelial in this system as evidenced by the maintenance of the epithelial markers E-cadherin, ZO-1, and Par complex components, suggesting that the role of Gata3 in prostate progenitor cells is different from the regulation of epithelial-mesenchymal transition reported in metastatic prostate cancer cells (Jiang et al., 2016; Wang et al., 2015).

An interesting consequence of these findings is that they provide a mechanism by which tissue hyperplasia occurs in the absence of cellular transformation. It is likely that this intermediate population generated by aberrant spindle orientation defects constitutes an epithelial cell population prone to oncogenic growth and dissemination upon transformation. Spindle orientation defects may therefore contribute to the hyperplastic and tumor progression phenotypes observed in the adult prostates and in other systems such as the skin and mammary gland in the absence of *Gata3* (Kaufman et al., 2003; Kouros-Mehr et al., 2006, 2008; Nguyen et al., 2013). Together, this work highlights the critical importance of regulating mitotic spindle orientation in progenitor cells to control the stepwise cellular differentiation process and maintain tissue architecture and homeostasis.

EXPERIMENTAL PROCEDURES

Mice

All experimental mice were kept in a C57BL/6 background. *Nkx3-1*^{Cre} (Thomsen et al., 2008), *Gata3*^{flox}, *Gata3*^{GFP} (Grote et al., 2006), *Rosa26*^{LacZ} (R26R) (Soriano, 1999), and *Rosa26dtTomato* (Madisen et al., 2010) mice were described previously. Immunodeficient SCID-beige mice were obtained from Charles River and kept in pathogen-free conditions. All animal procedures were approved by McGill University Animal Care Committee according to the Canadian Council on Animal Care guidelines for use of laboratory animals in biological research. Genotyping primers used are listed in Table S2. All histological analyses were performed on dorsal-lateral prostates.

In Situ Hybridization and β-Galactosidase Staining

Gata3 and *Nkx3-1* probe sequences have been previously described (Bhatia-Gaur et al., 1999; George et al., 1994). RNA probes for in situ hybridization were synthesized using T7 or SP6 RNA polymerase following the manufacturer's specifications (Roche). Tissues for in situ hybridization were fixed in 4% paraformaldehyde (PFA), passed through a sucrose gradient, embedded in optimal cutting temperature (OCT) medium, and sectioned at 12 μm. β-Galactosidase activity was detected by X-gal staining of whole-mount prostate tissue. In brief, whole prostates were fixed in Beta-Gal fixation solution, washed, stained using Beta-Gal staining solution for 1 hr at 37°C, and fixed in 4% PFA for 30 min.

qRT-PCR

Total RNA was extracted from control (n = 6) or *Nkx3-1*$^{Cre/+}$; *Gata3*$^{flox/flox}$ (n = 6) total or sorted prostate cells using an RNeasy mini kit (Qiagen) and reverse transcribed with Moloney murine leukemia virus (Invitrogen) according to the manufacturer's protocol. Real-time qPCR was performed using Green-2-go Mastermix (BioBasic) on a Realplex2 Mastercycler (Eppendorf). All primers used are listed in Table S2.

FACS Sorting and Analysis

Prostate tissue was dissected in cold PBS and 2% fetal bovine serum, minced, and digested at 37°C for 3 hr in collagenase/hyaluronidase solution (StemCell Technologies), followed by 5 min in 0.25% trypsin/EDTA and 10 min in 5 U/mL of dispase II with 0.1 mg/mL DNase I (Roche). The digested cells were passed through a 27-gauge needle and filtered through a 70-μm cell strainer. Single cells were stained on ice for 30 min with antibodies from BioLegend: CD45 (30-F11), Ter119 (TER-119), CD31 (MEC13.3), CD49f (GoH3), and CD24 (M1/69) (Wang et al., 2013). Fixable Viability dye (eBioscience) was used to select viable cells. For intracellular staining, cells were stained with CK5 antibody (Poly19055, BioLegend) and anti-rabbit Alexa Fluor 488 (Life Technologies) secondary antibody using a BD

Cytofix/Cytoperm Kit (BD Biosciences). FACS analysis and sorting was performed on a BD Fortessa and Aria Fusion apparatus (BD Biosciences). Unstained cells, single fluorochrome-stained cells, and cells stained as FMO (fluorescence minus one) were used to set up the machine and gating strategy. Data were analyzed using FlowJo software.

Immunohistochemistry

Immunofluorescence staining was performed on freshly frozen tissue embedded in OCT and sectioned to obtain 10- to 15-μm thick sections as described by Nguyen et al. (2013). Antibodies and dilutions used are listed in Table S3. Five mice of each genotype were used in IHC experiments.

Aurothiomalate Administration

Three control and four 2-week-old mice were injected intraperitoneally once daily with 80 mg/kg ATM in PBS (Sigma-Aldrich) for 4 weeks to inhibit the PRKCZ-PARD6B interaction in vivo. Solutions were light protected and stored at −20°C.

Microscopy and Image Analysis

H&E and bright-field whole-mount images were acquired with an Axioplan 2 microscope (Zeiss). Immunofluorescence images were acquired using an LSM3, LSM710, LSM780, or LSM800 confocal microscope (Zeiss). For quantification and spindle orientation analysis, images were captured using a spectral detector and linear unmixing was performed using Zen software (Zeiss).

Additional materials and methods are detailed in Supplemental Experimental Procedures.

SUPPLEMENTAL INFORMATION

Supplemental Information includes Supplemental Experimental Procedures, six figures, four tables, and one data file and can be found with this article online at http://dx.doi.org/10.1016/j.stemcr.2017.02.004.

AUTHOR CONTRIBUTIONS

M.E.R.S., A.H.T.N., M.T., S.V., and M.B. performed experiments. N.R.B. and M.P. contributed to microarray analysis. M.E.R.S., A.H.T.N., and M.B. conceived the project. M.E.R.S. and M.B. wrote the manuscript.

ACKNOWLEDGMENTS

We are grateful to members of the Bouchard laboratory for critical reading of the manuscript. We would like to thank the McGill Advanced BioImaging Facility (ABIF) for their technical support with spectral unmixing and confocal microscopy, as well as the Flow Cytometry platform of the McGill University Life Sciences Complex for cell sorting. This work was supported by grants from the Canadian Institutes of Health Research (CIHR; MOP-130460) and the Cancer Research Society (CRS, Canada) to M.B. M.B. holds a Senior Research Scholar Award from the Fonds de la Recherche du Québec-Santé (FRQS). M.E.R.S. was supported by a Graduate Studentship from Prostate Cancer Canada, and a Lloyd-Carr Harris Graduate Studentship from McGill University. A.H.T.N. was supported by a studentship from the CIHR and the McGill Integrated Cancer Research Training Program (MICRTP). M.T. was supported by a Dr. Gerald B. Price Fellowship (Cancer Research Society), and MICRTP and FRSQ postdoctoral fellowships.

Received: August 19, 2016
Revised: February 2, 2017
Accepted: February 3, 2017
Published: March 9, 2017

REFERENCES

Adachi, M., Hamazaki, Y., Kobayashi, Y., Itoh, M., Tsukita, S., Furuse, M., and Tsukita, S. (2009). Similar and distinct properties of MUPP1 and Patj, two homologous PDZ domain-containing tight-junction proteins. Mol. Cell Biol. *29*, 2372–2389.

Ahmed, S.M., and Macara, I.G. (2016). Mechanisms of polarity protein expression control. Curr. Opin. Cell Biol. *42*, 38–45.

Asselin-Labat, M.L., Sutherland, K.D., Barker, H., Thomas, R., Shackleton, M., Forrest, N.C., Hartley, L., Robb, L., Grosveld, F.G., van der Wees, J., et al. (2007). Gata-3 is an essential regulator of mammary-gland morphogenesis and luminal-cell differentiation. Nat. Cell Biol. *9*, 201–209.

Bergstralh, D.T., and St Johnston, D. (2014). Spindle orientation: what if it goes wrong? Semin. Cell Dev. Biol. *34*, 140–145.

Bhatia-Gaur, R., Donjacour, A.A., Sciavolino, P.J., Kim, M., Desai, N., Young, P., Norton, C.R., Gridley, T., Cardiff, R.D., Cunha, G.R., et al. (1999). Roles for Nkx3.1 in prostate development and cancer. Genes. Dev. *13*, 966–977.

Chatterjee, S.J., and McCaffrey, L. (2014). Emerging role of cell polarity proteins in breast cancer progression and metastasis. Breast Cancer *6*, 15–27.

Choi, N., Zhang, B., Zhang, L., Ittmann, M., and Xin, L. (2012). Adult murine prostate basal and luminal cells are self-sustained lineages that can both serve as targets for prostate cancer initiation. Cancer Cell *21*, 253–265.

Durgan, J., Kaji, N., Jin, D., and Hall, A. (2011). Par6B and atypical PKC regulate mitotic spindle orientation during epithelial morphogenesis. J. Biol. Chem. *286*, 12461–12474.

Dydensborg, A.B., Rose, A.A., Wilson, B.J., Grote, D., Paquet, M., Giguere, V., Siegel, P.M., and Bouchard, M. (2009). GATA3 inhibits breast cancer growth and pulmonary breast cancer metastasis. Oncogene *28*, 2634–2642.

Erdogan, E., Lamark, T., Stallings-Mann, M., Lee, J., Pellecchia, M., Thompson, E.A., Johansen, T., and Fields, A.P. (2006). Aurothiomalate inhibits transformed growth by targeting the PB1 domain of protein kinase Ciota. J. Biol. Chem. *281*, 28450–28459.

George, K.M., Leonard, M.W., Roth, M.E., Lieuw, K.H., Kioussis, D., Grosveld, F., and Engel, J.D. (1994). Embryonic expression and cloning of the murine GATA-3 gene. Development *120*, 2673–2686.

Grote, D., Souabni, A., Busslinger, M., and Bouchard, M. (2006). Pax 2/8-regulated Gata 3 expression is necessary for morphogenesis and guidance of the nephric duct in the developing kidney. Development *133*, 53–61.

Guilgur, L.G., Prudencio, P., Ferreira, T., Pimenta-Marques, A.R., and Martinho, R.G. (2012). *Drosophila* aPKC is required for mitotic spindle orientation during symmetric division of epithelial cells. Development *139*, 503–513.

Hao, Y., Du, Q., Chen, X., Zheng, Z., Balsbaugh, J.L., Maitra, S., Shabanowitz, J., Hunt, D.F., and Macara, I.G. (2010). Par3 controls epithelial spindle orientation by aPKC-mediated phosphorylation of apical Pins. Curr. Biol. *20*, 1809–1818.

Jiang, X., Chen, Y., Du, E., Yang, K., Zhang, Z., Qi, S., and Xu, Y. (2016). GATA3-driven expression of miR-503 inhibits prostate cancer progression by repressing ZNF217 expression. Cell Signal. *28*, 1216–1224.

Kaufman, C.K., Zhou, P., Pasolli, H.A., Rendl, M., Bolotin, D., Lim, K.C., Dai, X., Alegre, M.L., and Fuchs, E. (2003). GATA-3: an unexpected regulator of cell lineage determination in skin. Genes. Dev. *17*, 2108–2122.

Knoblich, J.A. (2010). Asymmetric cell division: recent developments and their implications for tumour biology. Nat. Rev. Mol. Cell Biol. *11*, 849–860.

Kouros-Mehr, H., Slorach, E.M., Sternlicht, M.D., and Werb, Z. (2006). GATA-3 maintains the differentiation of the luminal cell fate in the mammary gland. Cell *127*, 1041–1055.

Kouros-Mehr, H., Bechis, S.K., Slorach, E.M., Littlepage, L.E., Egeblad, M., Ewald, A.J., Pai, S.Y., Ho, I.C., and Werb, Z. (2008). GATA-3 links tumor differentiation and dissemination in a luminal breast cancer model. Cancer Cell *13*, 141–152.

Lim, K.C., Lakshmanan, G., Crawford, S.E., Gu, Y., Grosveld, F., and Engel, J.D. (2000). Gata3 loss leads to embryonic lethality due to noradrenaline deficiency of the sympathetic nervous system. Nat. Genet. *25*, 209–212.

Liu, J., Pascal, L.E., Isharwal, S., Metzger, D., Ramos Garcia, R., Pilch, J., Kasper, S., Williams, K., Basse, P.H., Nelson, J.B., et al. (2011). Regenerated luminal epithelial cells are derived from preexisting luminal epithelial cells in adult mouse prostate. Mol. Endocrinol. *25*, 1849–1857.

Madisen, L., Zwingman, T.A., Sunkin, S.M., Oh, S.W., Zariwala, H.A., Gu, H., Ng, L.L., Palmiter, R.D., Hawrylycz, M.J., Jones, A.R., et al. (2010). A robust and high-throughput Cre reporting and characterization system for the whole mouse brain. Nat. Neurosci. *13*, 133–140.

Marker, P.C., Donjacour, A.A., Dahiya, R., and Cunha, G.R. (2003). Hormonal, cellular, and molecular control of prostatic development. Dev. Biol. *253*, 165–174.

Morin, X., and Bellaiche, Y. (2011). Mitotic spindle orientation in asymmetric and symmetric cell divisions during animal development. Dev. Cell *21*, 102–119.

Nechiporuk, T., Klezovitch, O., Nguyen, L., and Vasioukhin, V. (2013). Dlg5 maintains apical aPKC and regulates progenitor differentiation during lung morphogenesis. Dev. Biol. *377*, 375–384.

Neumuller, R.A., and Knoblich, J.A. (2009). Dividing cellular asymmetry: asymmetric cell division and its implications for stem cells and cancer. Genes. Dev. *23*, 2675–2699.

Nguyen, A.H., Tremblay, M., Haigh, K., Koumakpayi, I.H., Paquet, M., Pandolfi, P.P., Mes-Masson, A.M., Saad, F., Haigh, J.J., and Bouchard, M. (2013). Gata3 antagonizes cancer progression in Pten-deficient prostates. Hum. Mol. Genet. *22*, 2400–2410.

Niessen, M.T., Scott, J., Zielinski, J.G., Vorhagen, S., Sotiropoulou, P.A., Blanpain, C., Leitges, M., and Niessen, C.M. (2013). aPKClambda controls epidermal homeostasis and stem cell fate through regulation of division orientation. J. Cell Biol. *202*, 887–900.

Oliaro, J., Van Ham, V., Sacirbegovic, F., Pasam, A., Bomzon, Z., Pham, K., Ludford-Menting, M.J., Waterhouse, N.J., Bots, M., Hawkins, E.D., et al. (2010). Asymmetric cell division of T cells upon antigen presentation uses multiple conserved mechanisms. J. Immunol. *185*, 367–375.

Ousset, M., Van Keymeulen, A., Bouvencourt, G., Sharma, N., Achouri, Y., Simons, B.D., and Blanpain, C. (2012). Multipotent and unipotent progenitors contribute to prostate postnatal development. Nat. Cell Biol. *14*, 1131–1138.

Pearson, H.B., Perez-Mancera, P.A., Dow, L.E., Ryan, A., Tennstedt, P., Bogani, D., Elsum, I., Greenfield, A., Tuveson, D.A., Simon, R., et al. (2011). SCRIB expression is deregulated in human prostate cancer, and its deficiency in mice promotes prostate neoplasia. J. Clin. Invest. *121*, 4257–4267.

Pignon, J.C., Grisanzio, C., Geng, Y., Song, J., Shivdasani, R.A., and Signoretti, S. (2013). p63-expressing cells are the stem cells of developing prostate, bladder, and colorectal epithelia. Proc. Natl. Acad. Sci. USA *110*, 8105–8110.

Rodriguez-Boulan, E., and Macara, I.G. (2014). Organization and execution of the epithelial polarity programme. Nat. Rev. Mol. Cell Biol. *15*, 225–242.

Shin, K., Straight, S., and Margolis, B. (2005). PATJ regulates tight junction formation and polarity in mammalian epithelial cells. J. Cell Biol. *168*, 705–711.

Soriano, P. (1999). Generalized lacZ expression with the ROSA26 Cre reporter strain. Nat. Genet. *21*, 70–71.

Thomsen, M.K., Butler, C.M., Shen, M.M., and Swain, A. (2008). Sox9 is required for prostate development. Dev. Biol. *316*, 302–311.

Wang, X., Kruithof-de Julio, M., Economides, K.D., Walker, D., Yu, H., Halili, M.V., Hu, Y.P., Price, S.M., Abate-Shen, C., and Shen, M.M. (2009). A luminal epithelial stem cell that is a cell of origin for prostate cancer. Nature *461*, 495–500.

Wang, Z.A., Mitrofanova, A., Bergren, S.K., Abate-Shen, C., Cardiff, R.D., Califano, A., and Shen, M.M. (2013). Lineage analysis of basal epithelial cells reveals their unexpected plasticity and supports a cell-of-origin model for prostate cancer heterogeneity. Nat. Cell Biol. *15*, 274–283.

Wang, J., Zhu, H.H., Chu, M., Liu, Y., Zhang, C., Liu, G., Yang, X., Yang, R., and Gao, W.Q. (2014). Symmetrical and asymmetrical division analysis provides evidence for a hierarchy of prostate epithelial cell lineages. Nat. Commun. *5*, 4758.

Wang, L., Song, G., Tan, W., Qi, M., Zhang, L., Chan, J., Yu, J., Han, J., and Han, B. (2015). MiR-573 inhibits prostate cancer metastasis by regulating epithelial-mesenchymal transition. Oncotarget *6*, 35978–35990.

Williams, S.E., Ratliff, L.A., Postiglione, M.P., Knoblich, J.A., and Fuchs, E. (2014). Par3-mInsc and Galphai3 cooperate to promote

oriented epidermal cell divisions through LGN. Nat. Cell Biol. *16*, 758–769.

Win, H.Y., and Acevedo-Duncan, M. (2008). Atypical protein kinase C phosphorylates IKKalphabeta in transformed non-malignant and malignant prostate cell survival. Cancer Lett. *270*, 302–311.

Wu, X., Xu, K., Zhang, L., Deng, Y., Lee, P., Shapiro, E., Monaco, M., Makarenkova, H.P., Li, J., Lepor, H., et al. (2011). Differentiation of the ductal epithelium and smooth muscle in the prostate gland are regulated by the Notch/PTEN-dependent mechanism. Dev. Biol. *356*, 337–349.

Wuidart, A., Ousset, M., Rulands, S., Simons, B.D., Van Keymeulen, A., and Blanpain, C. (2016). Quantitative lineage tracing strategies to resolve multipotency in tissue-specific stem cells. Genes. Dev. *30*, 1261–1277.

Xin, L., Ide, H., Kim, Y., Dubey, P., and Witte, O.N. (2003). In vivo regeneration of murine prostate from dissociated cell populations of postnatal epithelia and urogenital sinus mesenchyme. Proc. Natl. Acad. Sci. USA *100*, 11896–11903.

Zhang, K., Zhao, H., Ji, Z., Zhang, C., Zhou, P., Wang, L., Chen, Q., Wang, J., Zhang, P., Chen, Z., et al. (2016). Shp2 promotes metastasis of prostate cancer by attenuating the PAR3/PAR6/aPKC polarity protein complex and enhancing epithelial-to-mesenchymal transition. Oncogene *35*, 1271–1282.

Stem Cell Reports, Volume *8*

Supplemental Information

Lineage Specification from Prostate Progenitor Cells Requires Gata3-Dependent Mitotic Spindle Orientation

Maxwell E.R. Shafer, Alana H.T. Nguyen, Mathieu Tremblay, Sophie Viala, Mélanie Béland, Nicholas R. Bertos, Morag Park, and Maxime Bouchard

Supplemental Information

Supplemental Figures

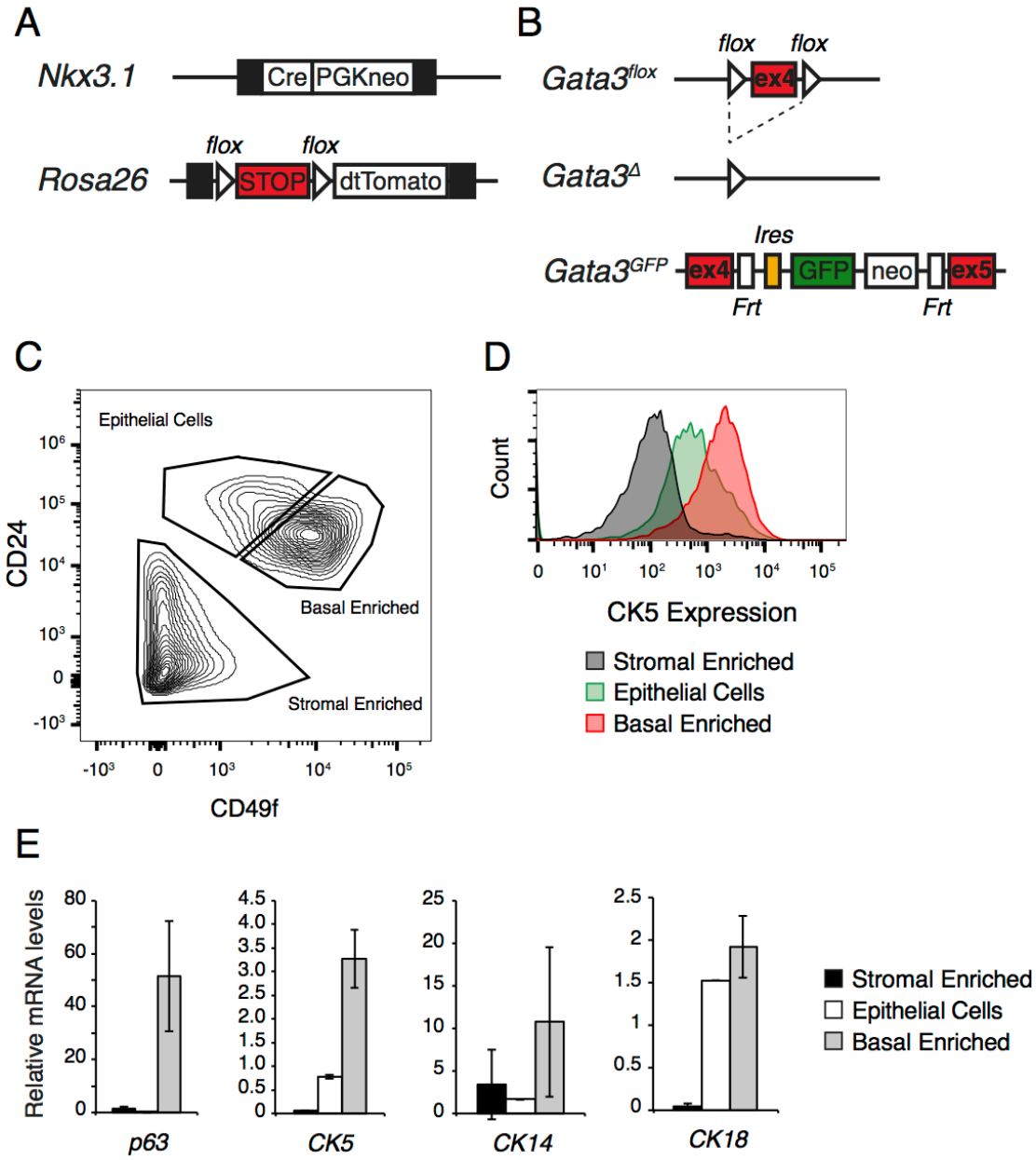

Figure S1. Lineage tracing constructs and enrichment of prostate basal cells by FACs. A) *Nkx3-1*^{Cre} was used to activate the *Rosa26*^{tdTomato} lineage tracing reporter construct. B) *Gata3* loci used in the study, including a floxed exon 4 which was removed by *Nkx3-1*^{Cre}, and an Ires GFP between exons 4 and 5 of *Gata3*. *Gata3*$^{\Delta}$ alleles were used to generate germ-line deletion mice. C) Representative fluorescent-activated cell sorting (FACS) plot of lineage negative (CD31-, Ter119-, Cd45-) cells from 2 week old prostate tissue showing stromal, epithelial and basal enriched cell populations based on CD24 and CD49f expression levels. D) Expression levels of CK5 in populations identified in C as measured by FACS. E) qRT-PCR of basal and luminal markers in FACS sorted populations. Error bars represent standard deviation from 3 technical replicates. FACS plots are representative of experiments from 3 individual prostates. See also Figure 1.

Figure S2. *Gata3*-deficient prostate branching defects are persistent in sexually mature mice. A) Ductal architecture of anterior, dorsal-lateral and ventral lobes from control and *Nkx3-1*^{Cre}*; Gata3*$^{flox/flox}$ prostates at 6 weeks old. Scale bar equals 1mm. See also Figure 2.

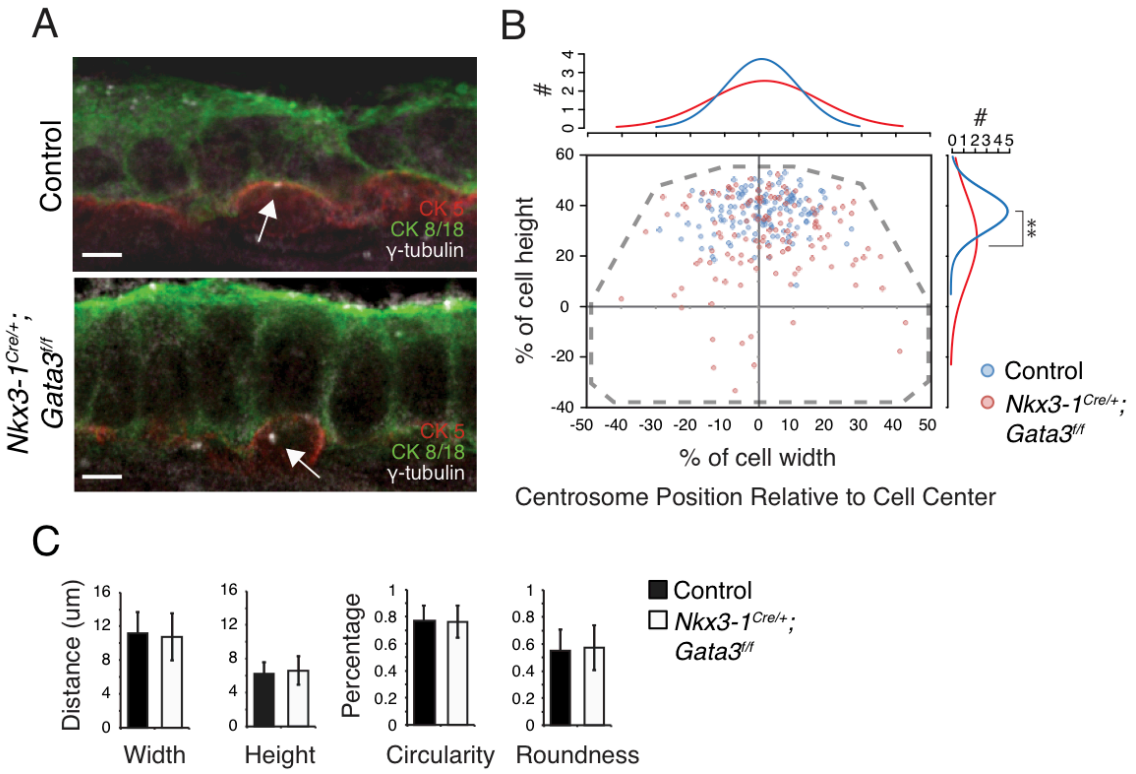

Figure S3. *Gata3* controls interphase centrosome localization in prostate progenitor cells. A) Localization of centrosomes (arrows) in control and *Nkx3-1*^{Cre}*; Gata3*$^{flox/flox}$ double positive progenitor cells by γ-tubulin immunofluorescence. Scale bars equal 5μm. B) Quantification of centrosome location relative to the centre of each cell in control and *Nkx3-1*^{Cre}*; Gata3*$^{flox/flox}$ progenitor cells. Location of each centrosome was represented as a percentage of the cell height or width. C) Size and shape of prostate progenitor cells in absence or presence of *Gata3*. Quantification is from 3 control and 3 *Nkx3-1*^{Cre}*; Gata3*$^{flox/flox}$ prostates**.** See also Figure 4.

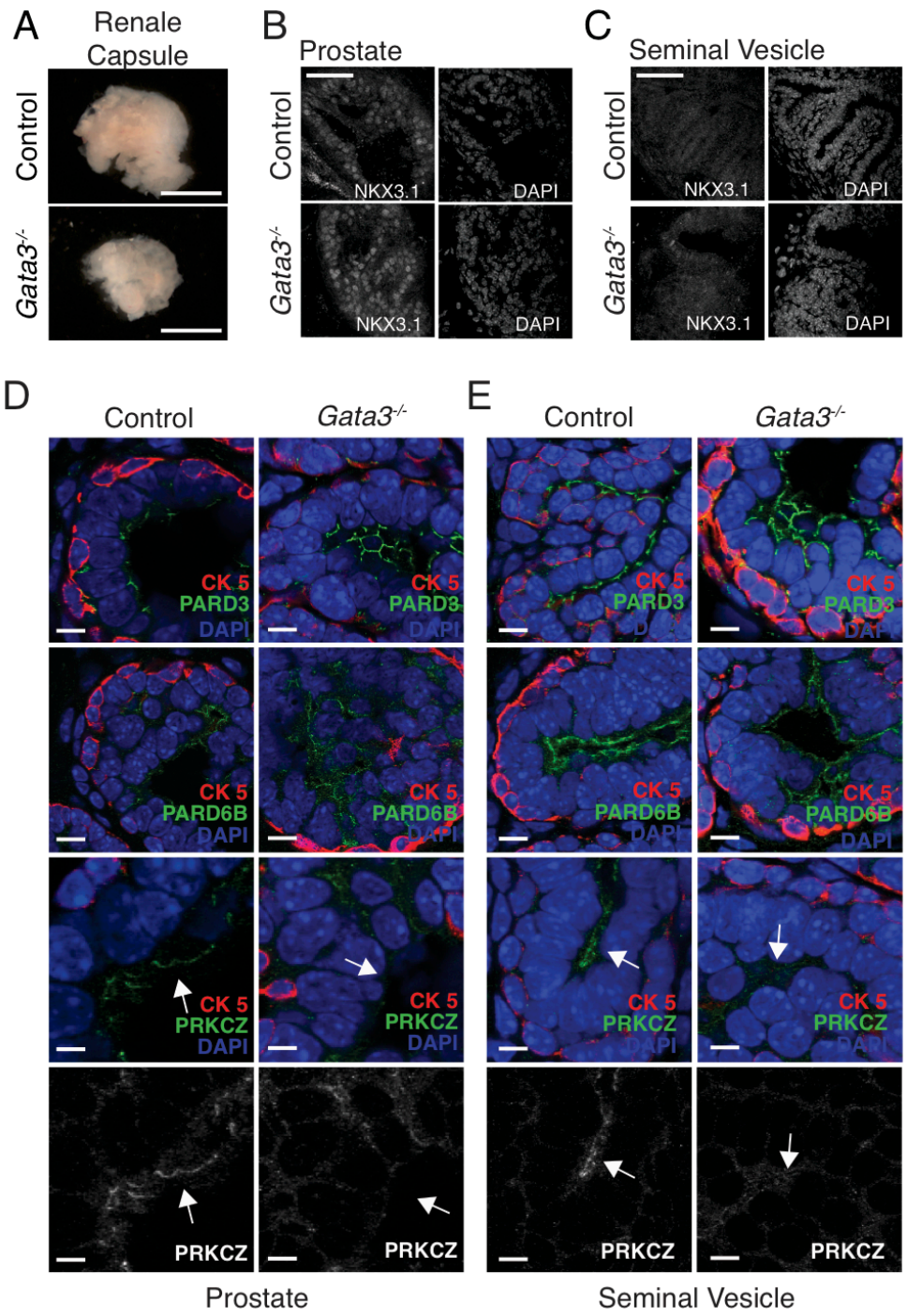

Figure S4. Germline deletion of *Gata3* affects prostate and seminal vesicle tissue. A) Urogenital tissue from drug rescued germline *Gata3* knockout and control embryos were grown under the kidney capsule of immunodeficient mice for 14 days. Scale bars are equal to 1mm. Presence of prostate (B) and seminal vesicle (C) after growth under the kidney capsule as detected by Nkx3-1 immunofluorescence staining and epithelial histology. Scale bars are equal to 50µm. D) Expression and localization of Pard3, Pard6b and aPKCz/i in drug rescued prostate tissue of germline *Gata3* knockout embryos grown under the kidney capsule. E) Expression and localization of Pard3, Pard6b and aPKC in drug rescued germline *Gata3* knockout grafted seminal vesicle tissue. Scale bars are equal to 10 µm. See also Figure 3. Arrows indicate the apical membrane.

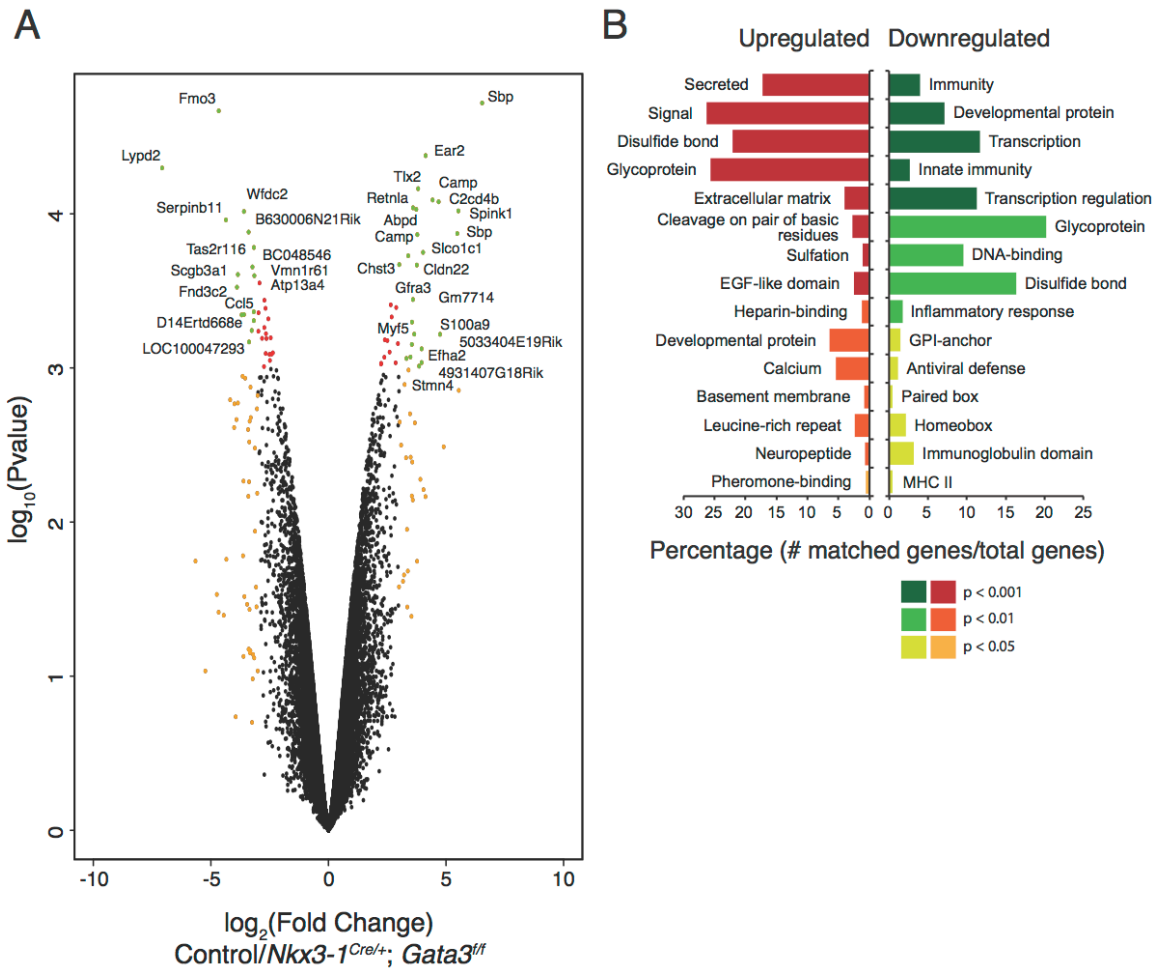

Figure S5. Transcriptional consequences of Gata3 deficiency. Microarray analysis was performed on epithelial cells obtained by laser capture micro dissection from 3 control and 3 *Nkx3-1*^{Cre}*; Gata3*$^{flox/flox}$ prostates. A) Volcano plot of transcripts differentially expressed between control and *Nkx3-1*^{Cre}*; Gata3*$^{flox/flox}$ prostate tissue. Colours represent transcripts which are log2(Fold Change)>3 (orange) or p-value<0.001 (red) or both (green, text labels). Labelled transcripts are also listed in Supplemental Table 1. B) Analysis of the differentially expressed transcripts for GO term enrichment using functional categories. Analysis was done using the most recent release of DAVID.

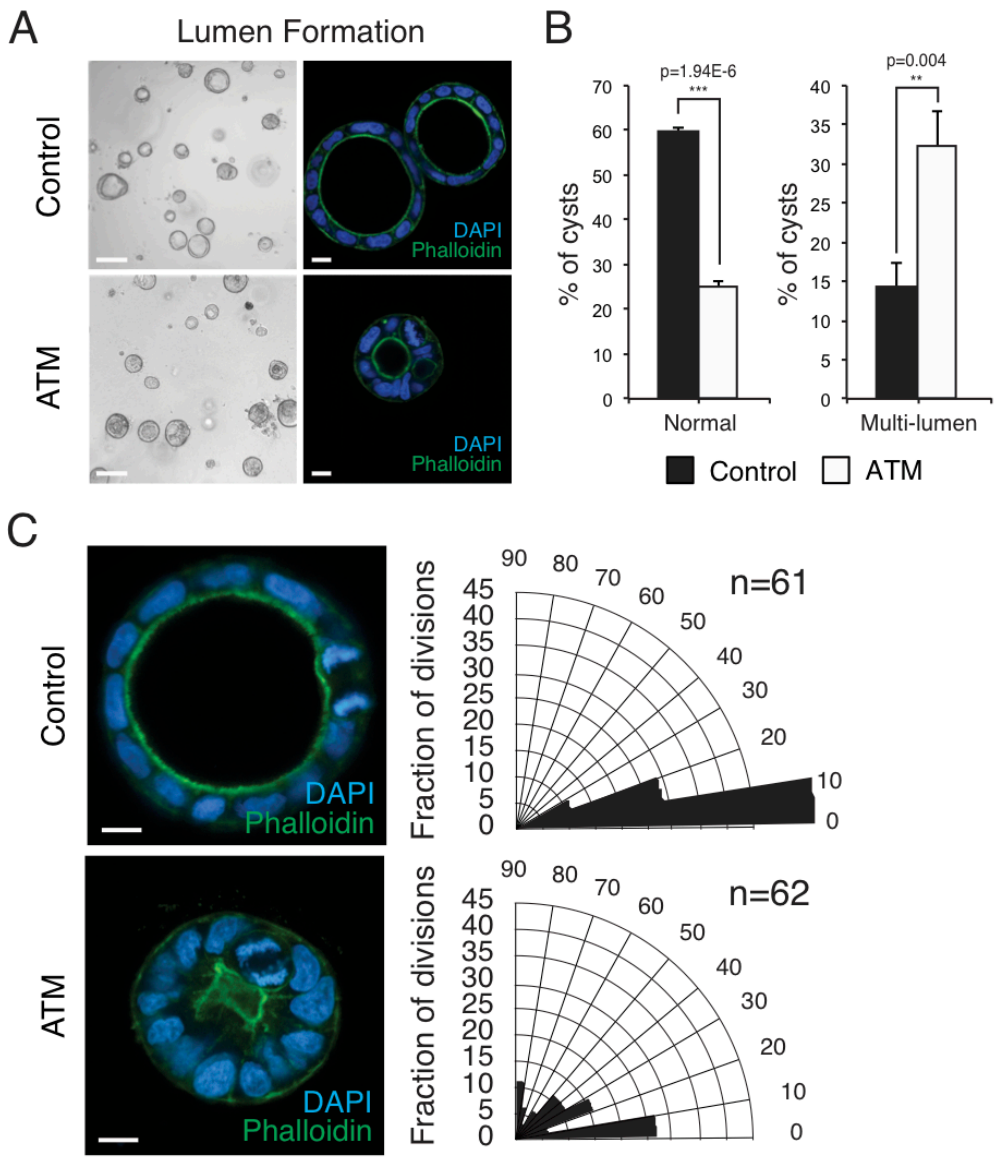

Figure S6. Mis-localization of aPKC causes epithelial defects in Caco-2 cysts. A) Effect of ATM on lumen formation in epithelial cysts by light microscopy and immunofluorescence using phalloidin and DAPI staining. Scale bars equal 100μm for bright field and 5μm for IHC. B) Quantification of normal or multi-lumen cysts after treatment with ATM. Error bars represent standard deviation of 3 independently treated samples of Caco-2 cysts. C) Measurement of spindle orientation in control and ATM-treated Caco-2 epithelial cysts. Spindle orientation was measured relative to the basal side of the cyst using DAPI and phalloidin staining. Scale bars are equal to 5μm. N represent the number of cell divisions measured. See also Figure 4.

Supplemental Table 1. Top regulated genes by microarray analysis of *Gata3* deficient epithelium ($(\log_2(\text{fold change}))>3$, p-value < 0.001).

Probe name	GeneSymbol	log2(Fold change)	P-value
A_55_P2078153	Sbp	6.535852	1.91E-05
A_51_P365516	Spink1	5.525317	9.58E-05
A_52_P294663	Sbp	5.479108	0.000134287
A_55_P1998471	S100a9	4.746343	0.000604859
A_55_P2054261	C2cd4b	4.686068	8.36E-05
A_51_P505521	Hist1h4i	4.449953	3.06E-05
A_55_P2039699	Camp	4.430271	8.13E-05
A_55_P1952618	Ear2	4.13247	4.19E-05
A_55_P2185832	Slco1c1	4.025487	0.000177908
A_55_P2428514	Retn	3.960925	0.000922969
A_51_P188281	Myf5	3.960323	0.000751629
A_55_P2045642	Stmn4	3.855307	0.000973621
A_55_P2164659	Tlx2	3.814866	6.87E-05
A_55_P2058201	Scgb2b20	3.780043	0.000136517
A_55_P2112459	Cldn22	3.758181	0.000215143
A_55_P2040653	Gm10824	3.73503	9.36E-05
A_51_P188281	Myf5	3.649437	0.000603499
A_51_P257951	Retnla	3.594639	9.14E-05
A_55_P1984103	Gfra3	3.592741	0.000359646
A_55_P2062078	Gm7714	3.553273	0.000504486
A_55_P2350665	5033404E19Rik	3.547267	0.000703888
A_55_P2007851	Micu3	3.487156	0.000849639
A_55_P2158102	Camp	3.392757	0.00018712
A_51_P127320	Cabs1	3.318	0.000867584
A_55_P2098067	Etos1	-3.151594	0.000252018
A_55_P1965574	BC048546	-3.169077	0.000165391
A_52_P638459	Ccl5	-3.174343	0.000493041
A_55_P2038217	Atp13a4	-3.174746	0.00043225
A_51_P445320	Tas2r116	-3.232771	0.000221261
A_55_P2015687	Phf11d	-3.263846	0.000571518
A_55_P2132982	Zfp987	-3.376576	0.000677995
A_55_P2421067	B630006N21Rik	-3.394777	0.000131393
A_55_P1972169	Vmn1r61	-3.593272	0.000450544
A_55_P1953341	Wfdc2	-3.59373	9.66E-05
A_55_P2033947	Fnd3c2	-3.691144	0.000452706
A_66_P130759	4631405J19Rik	-3.850394	0.000247762
A_51_P110341	Scgb3a1	-3.890031	0.000299347
A_51_P438853	Serpinb11	-4.35963	0.000109572
A_51_P269404	Fmo3	-4.664987	2.15E-05
A_51_P136521	Lypd2	-7.07352	5.04E-05

Supplemental Table 2. Primers used in this study

Gene	Usage	Forward Primer	Reverse Primer
Gata3 +/f/Δ	Genotyping	GTCAGGGCACTAAGGGTTGTT	TGGTAGAGTCCGCAGGCATTG
		TATCAGCGGTTCATCTACAGC	
Nkx3-1 Cre/+	Genotyping	GCG CGG TCT GGC AGT AAA AAC	CAG ATG GCG CGG CAA CAC C
R26 LacZ/+	Genotyping	ATACTGTCGTCGTCCCCTCAAACTG	TTCAACCACCGCACGATAGAGATT
Gata3 (exon 4)	qRT-PCR	TTATCAAGCCCAAGCGAAG	TGGTGGTGGTCTGACAGTTC
p63 (Tpr63)	qRT-PCR	TCGATGTGTCCTTCCAGCAGTCAA	TGTAGACAGGCATGGCACGGATAA
CK5 (Krt5)	qRT-PCR	GAGATCGCCACCTACAGGAA	TCCTCCGTAGCCAGAAGAGA
CK14 (Krt14)	qRT-PCR	CCTCTGGCTCTCAGTCATCC	CCTCTGGCTCTCAGTCATCC
CK18 (Krt18)	qRT-PCR	CGAGGCACTCAAGGAAGAAC	AATCTGGGCTTCCAGACCTT

Supplemental Table 3. Antibodies used in this study

Antibody	Source	Dilution
CK5 (Chicken)	Covance, SIG-3475	1:200
CK8 & CK18 (Guinea Pig)	Fitzgerald, 20R-CP004	1:200
Gata3 (Rabbit)	Santa Cruz, sc-9009	1:50
E-cadherin (Mouse)	BD Biosciences	1:200
ZO-1 (Rat)	Chemicon	1:200
Phospho-H3 (Rabbit)	Millipore, 06-570	1:100
γ-tubulin (Goat)	Santa Cruz, sc-7396	1:100
Pard3 (Rabbit)	Millipore, 07-330	1:100
Pard6b (Rabbit)	Santa Cruz, sc-67393	1:50
aPKCz/i (Rabbit)	Santa Cruz, SC-216	1:50
Nkx3-1 (Rabbit)	Santa Cruz, sc-25406	1:50
Phalloidin	Life Technologies	1:500

Supplemental Table 4. Spindle orientation chi-squared test results

Condition 1	Condition 2	Chi-squared p-value	Level of significance	Figure
All Cells (Control)	All Cells (Nkx3-1Cre;Gata3f/f)	<0.001	****	2E
Basal Cells (Control)	Basal Cells (Nkx3-1Cre;Gata3f/f)	<0.001	****	2E
Luminal Cells (Control)	Luminal Cells (Nkx3-1Cre;Gata3f/f)	<0.001	****	2E
Double Positive Cells (Control)	Double Positive Cells (Nkx3-1Cre;Gata3f/f)	<0.001	****	2E
Caco2 (Control)	Caco2 (ATM Treated)	<0.001	****	4A
All Cells (Control)	All Cells (ATM Treated)	<0.001	****	4C
Basal Cells (Control)	Basal Cells (ATM Treated)	0.0278	*	4C
Luminal Cells (Control)	Luminal Cells (ATM Treated)	<0.001	****	4C
Double Positive Cells (Control)	Double Positive Cells (ATM Treated)	0.2468	ns	4C

Supplemental Materials and Methods

Drug rescue and kidney capsule implantation

To generate germline *Gata3* mutant urogenital tissue, *Gata3*$^{-/-}$ embryos, which normally die around E11.5, were grown until E18.5 using a modified version of a drug rescue regimen (Kaufman et al., 2003; Lim et al., 2000). E5.5-E7.5, pregnant *Gata3*$^{+/-}$ dams were given fresh water daily containing 100 μg/ml isoproterenol, 1 mg/ml DOPA and 2 mg/ml ascorbic acid in a light protected container (Sigma). E18.5 male urogenital systems (including the urethra, seminal vesicles and prostate) were then transferred under the kidney capsule of a male immunodeficient mouse with a sub-cutaneous testosterone plug for 14 days as previously described (Nicholson et al., 2013).

Laser capture microdissection and microarray analysis

Prostate epithelial cells were isolated by laser capture micro-dissection of cryo-sectioned 2-week old prostates. Epithelial ducts were captured by infrared laser using an ArcturusXT Microdissection System (Applied Biosystems). RNA was extracted and subjected to two rounds of linear amplification before labeling and hybridization to Agilent microarray chips. Microarray chips were scanned on a Microarray Scanner Model G2505B (Agilent Technologies).

Microarray data were normalized, and differential expression was performed using the LIMMA package in FlexArray (Genome Quebec). The volcano plot was generated using R Studio and GO term enrichment was done using the most recent release of DAVID (6.8 Beta) (Huang da et al., 2009a, b).

Aurothiomalate administration in vitro

Caco-2 cells were grown in DMEM (10% FBS) (Gibco) with appropriate antibiotics. Cysts were produced by plating Caco-2 cells in matrigel (Corning) and grown for 7-10 days. For inhibition of the aPKC-Par6b interaction, aurothiomalate (ATM) was added to the media for the duration of cyst growth.

Image analysis

Proliferation/apoptosis, spindle orientation analysis, cell lineage quantification, basal cell centriole localization, and aPKC fluorescence intensity were all and analyzed using Fiji (ImageJ) software. Proliferation/apoptosis and cell lineage quantification was performed using the Cell Counter plugin from representative fields of view (Fiji). DAPI positive cells were first identified, then each was assigned as CK5+, CK8/18+ or double positive. Counts were standardized for the circumference of the each duct quantified. Centriole localization was performed by first straightening the prostate duct along the basal side using Fiji, followed by calculation of the size, position and shape of both the basal cells and their centrioles.

Statistical analysis

For differences in proliferation, apoptosis, number of cells per ductal boundary and centrosome location, statistical significance was determined by student's t-test. Statistical analysis of spindle orientation was determined by chi-squared analysis as previously described (Williams et al., 2014), by separating spindle orientations measurements into 3 bins; 0-20°, 20-70° or 70-90°. Statistical analyses were performed using Prism software (GraphPad).

Supplementary References

Bhatia-Gaur, R., Donjacour, A.A., Sciavolino, P.J., Kim, M., Desai, N., Young, P., Norton, C.R., Gridley, T., Cardiff, R.D., Cunha, G.R.*, et al.* (1999). Roles for Nkx3.1 in prostate development and cancer. Genes & development *13*, 966-977.

George, K.M., Leonard, M.W., Roth, M.E., Lieuw, K.H., Kioussis, D., Grosveld, F., and Engel, J.D. (1994). Embryonic expression and cloning of the murine GATA-3 gene. Development *120*, 2673-2686.

Huang da, W., Sherman, B.T., and Lempicki, R.A. (2009a). Bioinformatics enrichment tools: paths toward the comprehensive functional analysis of large gene lists. Nucleic acids research *37*, 1-13.

Huang da, W., Sherman, B.T., and Lempicki, R.A. (2009b). Systematic and integrative analysis of large gene lists using DAVID bioinformatics resources. Nature protocols *4*, 44-57.

Kaufman, C.K., Zhou, P., Pasolli, H.A., Rendl, M., Bolotin, D., Lim, K.C., Dai, X., Alegre, M.L., and Fuchs, E. (2003). GATA-3: an unexpected regulator of cell lineage determination in skin. Genes & development *17*, 2108-2122.

Lim, K.C., Lakshmanan, G., Crawford, S.E., Gu, Y., Grosveld, F., and Engel, J.D. (2000). Gata3 loss leads to embryonic lethality due to noradrenaline deficiency of the sympathetic nervous system. Nature genetics *25*, 209-212.

Nicholson, T.M., Uchtmann, K.S., Valdez, C.D., Theberge, A.B., Miralem, T., and Ricke, W.A. (2013). Renal capsule xenografting and subcutaneous pellet implantation for the evaluation of prostate carcinogenesis and benign prostatic hyperplasia. Journal of visualized experiments : JoVE.

Williams, S.E., Ratliff, L.A., Postiglione, M.P., Knoblich, J.A., and Fuchs, E. (2014). Par3-mInsc and Galphai3 cooperate to promote oriented epidermal cell divisions through LGN. Nature cell biology *16*, 758-769.